REVIEW

Check for updates

Photoresponsive lanthanide luminescent materials

Lingna Su,[a] Xiao Liu,*[a] Qingyu Niu[a] and Zhiqiang Li [ID] *[ab]

Lanthanide luminescent materials have attracted great attention in the last few decades due to their intriguing optical properties, such as large Stokes shift, long excited state lifetimes, high quantum efficiencies, abundant emission spectra, and high color purity. Stimuli-responsive materials are smart materials that can sense and respond to surrounding stimuli. The combination of stimuli-response with the unique luminescent properties of lanthanides has great potential for numerous applications. Compared to other stimuli, light irradiation offers many advantages, such as cleanliness, easy availability, high efficiency, and remoteness. This review focuses on the construction and response mechanism of photoresponsive lanthanide luminescent materials. Furthermore, various important applications in luminescent actuators, photoswitches, intelligent anticounterfeiting, and theranostics are also highlighted in detail.

1. Lanthanide luminescent materials

Lanthanide elements located in the sixth period and IIIB group in the periodic table consist of 15 elements from lanthanum (atomic number 57) to lutetium (atomic number 71), and their unique electronic configuration is [Xe] $4f^{n-1}5d^{0-1}6s^2$ ($n = 1$–15).[1–4] The lanthanide elements have similar chemical properties due to their nearly identical outermost electron arrangements. The valence states of lanthanide elements can range from +2 to +4, with +3 being the most common, characterized by the electron configurations [Xe]$4f^{0-14}$, which indeed produce a diverse range of electronic levels.[5–7] Therefore, lanthanide materials display distinctive optical, magnetic, and electrical properties, showing a wide range of applications, including but not limited to photonic devices, renewable energy, biomedical devices, industrial products, and display devices.[8–11]

As an important branch, the luminescence of lanthanide (Ln^{3+}) ions originated from transitions inside the 4f shell, thus intraconfigurational f–f transitions have become a research hot spot.[12,13] Different Ln^{3+} ions emit luminescence of various colors because of the different energy gaps of radiative transitions. For instance, Eu^{3+} emits red light, Tb^{3+} emits green light, Sm^{3+} emits orange light, Tm^{3+} emits blue light, and Dy^{3+} emits white or near-white light. Additionally, Pr^{3+}, Nd^{3+}, Dy^{3+}, Ho^{3+}, Er^{3+}, Tm^{3+}, and Yb^{3+} all emit radiation in near-infrared (NIR) light.[14–16] The emission spectra of Ln^{3+} ions cover a wide range, including the ultraviolet (UV), visible (400–800 nm), and NIR (800–1700 nm) regions, which are widely recognized as valuable emitting sources.[17,18] Due to the shielding effect of the partially filled 4f shell by the closed $5s^2$ and $5p^6$ shells, the emission

[a] School of Chemical Engineering and Technology, Hebei University of Technology, GuangRong Dao 8, Hongqiao District, Tianjin 300130, P. R. China. E-mail: 2023925@hebut.edu.cn, zhiqiangli@hebut.edu.cn

[b] Key Laboratory of Advanced Energy Materials Chemistry (Ministry of Education), Nankai University, Tianjin 300071, China

Lingna Su is a master's student at Hebei University of Technology. She received her bachelor's degree from Datong University. Her research interests are focused on constructing lanthanide luminescent materials.

Lingna Su

Xiao Liu received her PhD degree under the supervision of Prof. Zhiqiang Li at Hebei University of Technology in 2023. Then, she joined Hebei University of Technology as a post-doctoral researcher. Her research interests focus on the design and synthesis of lanthanide luminescent materials.
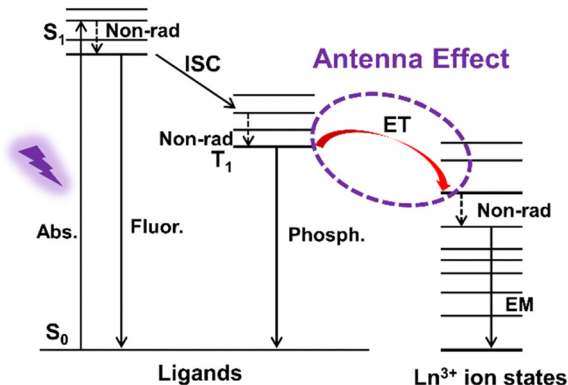
Xiao Liu

Fig. 1 Intramolecular energy transfer mechanism for the lanthanide materials.
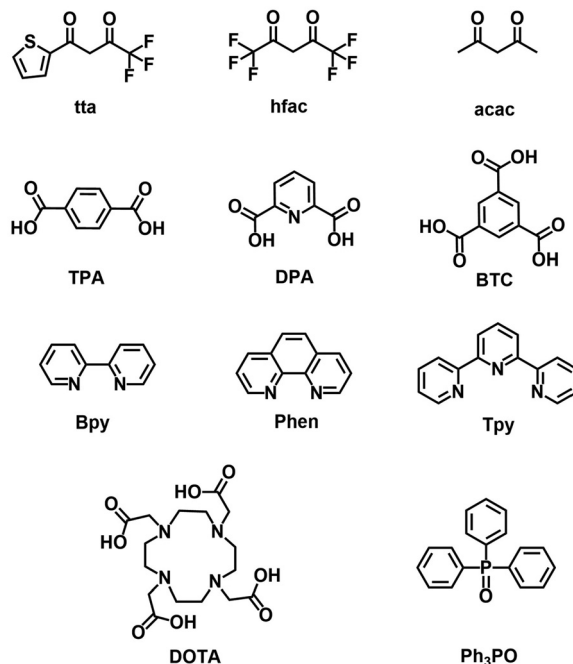

Fig. 2 Chemical structure of common organic ligands: 2-thiophenyltrifluoroacetone (tta), hexafluoroacetylacetone (hfac), acetylacetone (acac), terephthalic acid (TPA), pyridine-2,6-dicarboxylic acid (DPA), 1,3,5-benzenetricarboxylic acid (BTC), 2,2′-bipyridine (Bpy), 1,10-phenanthroline (Phen), terpyridyl (Tpy), 2,2′,2″-(1,4,7,10-tetraazacyclo-dodecane-1,4,7-triyl)triaceticacid (DOTA), and triphenylphosphine oxide (Ph₃PO).

wavelengths of Ln^{3+} ions are hardly affected by ligands in the first and second coordination sphere, which in particular results in narrow emission bands and long excited lifetimes.[19]

However, all Ln^{3+} ions have low absorption cross-sections (absorption coefficients ε, < 10 L mol^{-1} cm^{-1}), so only a limited amount of radiation is absorbed through direct excitation in the 4f energy level, resulting in weak luminescence.[20] In order to solve this problem, coordinating Ln^{3+} ions with organic ligands offers a viable approach, which can resolve the weak light absorption caused by the forbidden f–f transitions. Upon exposure to external UV light, the organic ligands absorb energy and transition from the ground state (S_0) to the excited singlet state (S_1), then transfer the energy to the excited triplet state (T_1) through the intersystem crossing (ISC). In addition, the energy is transferred from the triplet state to the excited state of the central Ln^{3+} ions *via* nonradiative transitions (Non-rad.). Finally, Ln^{3+} ions emit their characteristic luminescence through radiative transitions from the excited state to the ground state (Fig. 1).[21] It is important to note that not all organic ligands can sensitize Ln^{3+} ions, which relies on the energy gap of the lowest excited triplet state T_1 and the 4f excited state of the Ln^{3+} ions. Effective transfer can only occur if the energy gap between

is in the appropriate range. Commonly used organic ligands include β-diketones (2-thiophenyltrifluoroacetone, hexafluoroacetylacetone, and acetylacetone), aromatic carboxylic acids (terephthalic acid, pyridine-2,6-dicarboxylic acid, and 1,3,5-benzenetricarboxylic acid), heterocyclic compounds (2,2′-bipyridine, 1,10-phenanthroline, and terpyridyl), macrocyclic ligands (macrocyclic polyether and macrocyclic polyketone), and compounds containing phosphoryl groups (triphenylphosphine oxide) (Fig. 2).[22–27] Luminescence from lanthanide materials with narrow-band, large

Qingyu Niu

Qingyu Niu is a graduate student under the supervision of Prof. Zhiqiang Li at Hebei University of Technology. His current research focuses on the design and synthesis of supramolecular luminescent materials.

Zhiqiang Li

Zhiqiang Li received his BS at Inner Mongolia University in 2009 and his PhD at Nankai University under the guidance of Prof. Yu Liu in 2014. From 2017 to 2019, he worked as a Postdoctoral Research Fellow under the supervision of Prof. Banglin Chen at the University of Texas at San Antonio. Currently, he is a Full Professor of School of Chemical Engineering and Technology, Hebei University of Technology. His current research interest is the self-assembly of lanthanide-containing hybrid luminescent materials.

Stokes shift and longer decay time,[28,29] is obtained by the so-called "antenna effect",[30,31] showing various optical applications.

2. Stimuli-responsive lanthanide luminescent materials

Stimuli-responsive materials are smart materials that undergo chemical and physical changes in response to external stimuli.[32–34] External stimuli can be classified into physical stimuli, such as light,[35] electricity,[36] magnetism,[37] mechanical force,[38] humidity,[39] and temperature,[40] and chemical stimuli,[41] such as pH,[42] redox,[43] and ions.[44] These interactive, adaptive, and self-regulating features make them attractive as smart and multifunctional materials in various fields. Stimuli-responsive lanthanide luminescent materials,[45,46] which achieve structure or luminescence signal changes in response to external stimuli, are one of the most important subclasses of lanthanide luminescent materials, showing potential applications in the fields of medical diagnosis,[47,48] chemical sensors,[49,50] biomimetic soft robotics,[51,52] data storage,[53] and security technologies.[54] The response mechanism of various stimuli-responsive materials can be categorized as energy transfer and competitive coordination, *etc.* Energy transfer encompasses interactions between the two Ln^{3+} ions, as well as between the ligand and the Ln^{3+} ion. Competitive coordination encompasses competition between the water molecule and the organic ligand, as well as competition between other metal ions and the Ln^{3+} ion. Next, some representative examples of stimuli-responsive lanthanide luminescent materials will be discussed.

2.1. Energy transfer

2.1.1. Thermo-responsive. With increasing temperature, the luminescence intensity of Ln^{3+} ions typically decreases due to thermal activation of the non-radiative deactivation.[55,56] However, co-doping Ln^{3+} ions can result in a luminescence increase of one Ln^{3+} ion and a decrease of the other Ln^{3+} ion, or a luminescence dramatic decrease of one Ln^{3+} ion and a slight decrease of the other Ln^{3+} ion, which is due to energy transfer between the two Ln^{3+} ions.[57] Qian and Chen *et al.* developed a mixed-lanthanide metal–organic framework (LnMOFs) ($Eu_{0.0069}$-$Tb_{0.9931}$-DMBDC, DMBDC = 2,5-dimethoxy-1,4-benzenedicarboxylic acid), and constructed a high-sensitivity luminescent thermometer using the temperature-dependent energy transfer between Tb^{3+} and Eu^{3+} in $Eu_{0.0069}Tb_{0.9931}$-DMBDC (Fig. 3).[58] Lanthanide luminescence temperature sensors have the advantages of adjustable size, easy modification, and non-invasiveness. Therefore, the development and utilization of lanthanide luminescent temperature sensors have gained increasing attention, and show great potential in industry, medicine, and daily life.

2.1.2. pH-responsive. pH stimulation causes protonation or deprotonation of organic ligands, which in turn affects the efficiency of energy transfer from the ligand to the Ln^{3+} ion, ultimately affecting the luminescence of lanthanide materials.[59,60] Qian *et al.* reported a nanoscale MOF (UiO-67-bpydc, bpydc = 2,2-bipyridine-5,5-dicarboxylic acid) with a stable structure and good
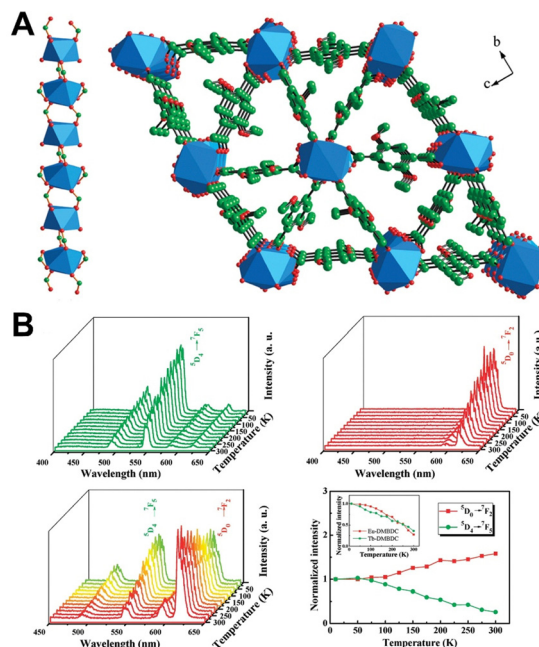

Fig. 3 (A) Structure of Tb-DMBDC. (B) Emission spectra of Tb-DMBDC, Eu-DMBDC, and $Eu_{0.0069}Tb_{0.9931}$-DMBDC recorded between 10 and 300 K, and the temperature dependence of integrated intensities of $Eu_{0.0069}Tb_{0.9931}$-DMBDC. Reproduced with permission from ref. 58. Copyright: 2012, American Chemical Society.

biocompatibility (Fig. 4).[42] The bipyridine can anchor and sensitize Eu^{3+} ions. The luminescence intensity of Eu^{3+} ions at 615 nm showed an obvious increase with increasing pH (pH = 1.06–10.99), which can be utilized as an effective luminescent pH sensor.

2.1.3. Redox-responsive. Some organic ligands undergo redox reactions in lanthanide luminescent materials. This can alter the triplet energy levels of the organic ligands and impact the energy transfer from organic ligands to Ln^{3+} ions, leading to an obvious change in luminescence intensity.[61,62] Chang *et al.* reported a lanthanide luminescent probe based on macrocyclic ligands for the detection of hydrogen peroxide (H_2O_2) in living systems (Fig. 5).[63] The probes could be dissociated under H_2O_2 to generate phenol and aniline antenna molecules that can effectively sensitize Tb^{3+} ions and maintain excellent luminescence performance. With the development of life sciences, redox gases (*e.g.*, hydrogen sulfide, carbon monoxide, hydrogen peroxide) are often of great significance to the activities of living systems. Therefore, accurate sensing of these types of gases based on lanthanide luminescent materials has become a research hotspot.

2.2. Competitive coordination

2.2.1. Humidity-responsive. It is widely known the luminescence of lanthanide materials can be significantly quenched under aqueous conditions because of the nonradiative transitions caused by coupling of –OH high-frequency stretching vibrations with Ln^{3+} ions.[64,65] Tanas *et al.* designed an effective and reliable humidity sensor based on LnMOFs ([$Eu(H_2O)_2$-$(mpca)_2Eu(H_2O)_6M(CN)_8]\cdot nH_2O$, mpca = 2-pyrazine-5-methyl-

This journal is © The Royal Society of Chemistry 2024

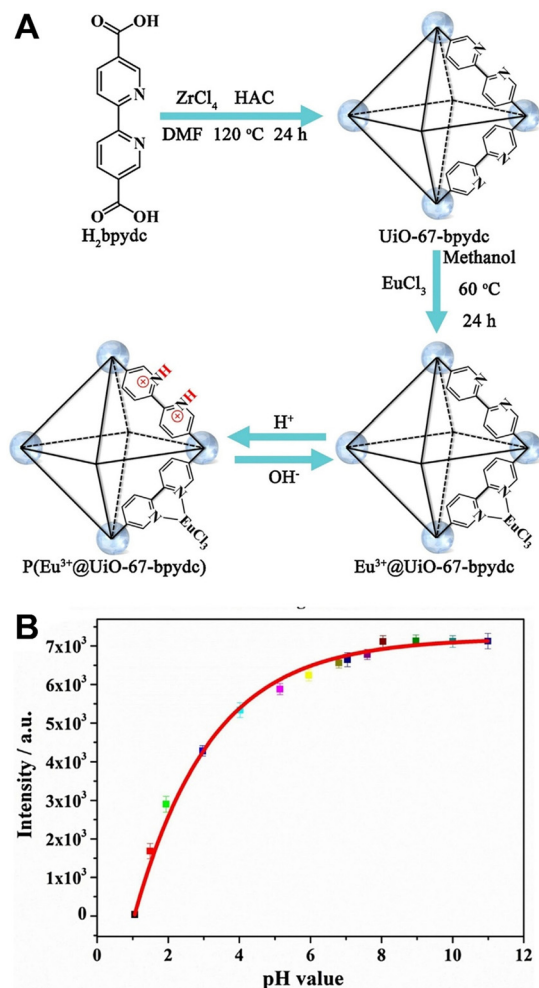*J. Mater. Chem. C*, 2024, **12**, 10759–10774 | **10761**

Fig. 4 (A) Protonation and deprotonation of Eu@UiO-67-bpydc. (B) The relationship between the emission intensity at 615 nm and the pH value. Reproduced with permission from ref. 42 Copyright: 2018, Elsevier.
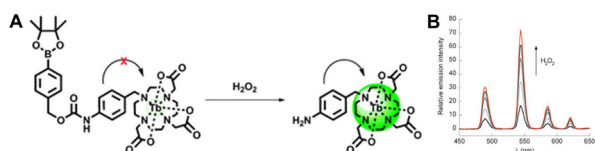

Fig. 5 (A) Chemical structure and response mechanism of luminescent probes. (B) Emission spectra at different concentrations of H_2O_2. Reproduced with permission from ref. 63 Copyright: 2010, the Royal Society of Chemistry.

carboxylate, M = Mo or W) with highly hydrophilic open pores.[39] The luminescence intensity of LnMOFs showed a fast response to water with high sensitivity and reproducibility (Fig. 6). Humidity and water vapor can significantly affect packaging materials and moisture-sensitive components. Therefore, precise monitoring of relative humidity is essential for global transportation and daily storage.

2.2.2. Ion-responsive. Competitive coordination occurs in the lanthanide luminescent system when adding other metal
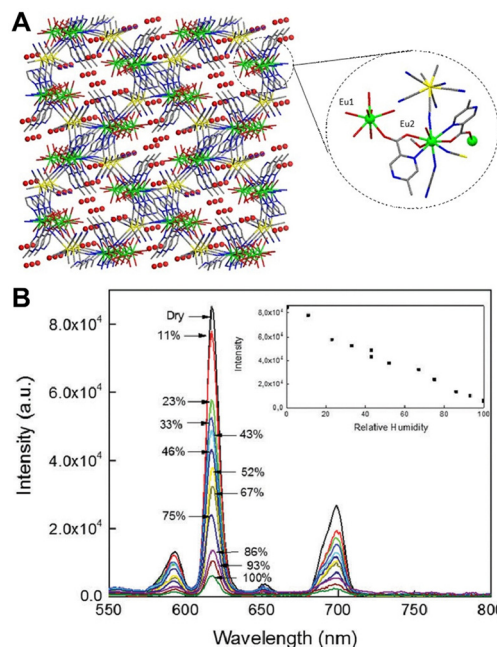

Fig. 6 (A) Structure of $[Eu(H_2O)_2(mpca)_2Eu(H_2O)_6M(CN)_8]\cdot nH_2O$. (B) Emission spectra at different humidity. Inset: Emission intensity at 617 nm as a function of humidity. Reproduced with permission from ref. 39 Copyright: 2017, the Royal Society of Chemistry.

ions with stronger affinity to the ligand. This results in the replacement of Ln^{3+} ions by other metal ions, disrupting the coordination bonds and causing luminescence quenching.[7,49,66] He *et al.* grafted iminodiacetate (IDA) onto poly(*N,N*-dimethyl-acrylamide) chains as a ligand, and then crosslinked the chains to form a hydrogel by coordination interaction between IDA and Eu^{3+} ion (Fig. 7).[67] When adding competing ions (Fe^{3+}, Zn^{2+}, and Cu^{2+}), the coordination bond between Eu^{3+} and the ligand was broken, and luminescence quenching as well as a gel–sol transition were observed. Ion-responsive lanthanide luminescent hydrogels offer a novel approach to construct intelligent optical materials.

3. Photoresponsive lanthanide luminescent materials

Despite many advances in stimuli-responsive lanthanide luminescent materials, there are still some challenges. First, some invasive stimuli can cause irreversible luminescence quenching. For example, the addition of transition metal ions (Fe^{3+}, Fe^{2+}, Cu^{2+}, and so on) triggers the gel–sol transition, but the luminescence signal also irreversibly disappears during this process because the organic ligand coordinates with these ions.[67] Luminescence on–off switching can be achieved to some extent by pH stimulation, which is based on the protonation or deprotonation of organic ligands. However, its fatigue resistance can only be maintained for a few cycles.[68–70] An excess of alkali may cause Ln^{3+} ions to precipitate as hydroxides or oxides, resulting in irreversible luminescence quenching.[71]
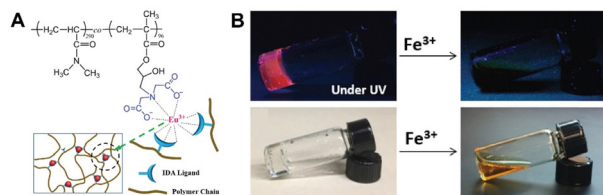
Fig. 7 (A) Schematic illustration and chemical structure of luminescent hydrogels with Eu^{3+} as the cross-linking points. (B) Fe^{3+}-induced luminescence quenching and gel–sol transition under UV light (upper) and daylight (lower). Reproduced with permission from ref. 67. Copyright: 2018, Wiley-VCH.

Second, certain stimuli have the potential to harm biological tissues in biomedical applications, such as tumor diagnosis and targeted drug delivery. For instance, a pH-responsive anticancer system may release drugs in the acidic endolysosomes of normal cells, causing side effects.[72,73] Direct heating can cause thermal damage to the physiological functions of normal tissues, whereas photothermal conversion can accurately and precisely stimulate specific locations on command.[74] Third, obtaining certain stimuli, such as strong magnetic and electric fields, may be challenging in reality. Forth, the redox process may produce by-products and alter the valence state of Ln^{3+} ions.[75,76]

In contrast, light irradiation has emerged as an ideal stimulus because of its high spatial/temporal resolution, controllability, rapidness, cleanliness, and handiness.[77,78] Researchers have combined photoresponse with lanthanide luminescent materials by introducing various photoresponsive molecules into lanthanide systems.[79–82] This has resulted in the development of a range of functional photoresponsive lanthanide luminescent materials including in luminescent actuators, photoswitches, intelligent anticounterfeiting, and theranostics. Common photoresponsive molecules can be divided into different types (Fig. 8).

3.1. Photoresponsive molecules and mechanisms

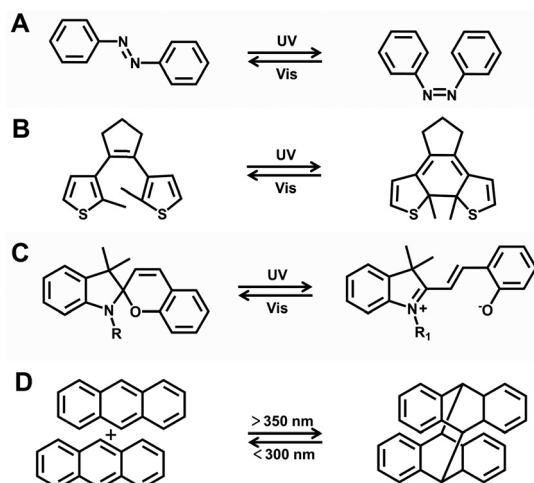**3.1.1. *Trans*/*cis* isomerization.** Azobenzene, as a promising photo-isomerization molecule, has been extensively studied in photoresponsive systems, and its isomerization process does not produce by-products. *Trans*(E)-azobenzene irradiated with UV light undergoes geometric isomerization around the N=N bond to produce *cis*(Z)-azobenzene. When irradiated with visible light, it isomerizes back to E-azobenzene (Fig. 8A).[83,84]

3.1.2. Ring-closure/ring-opening isomerization. Photochromism is a chemical reaction that occurs when compound A is irradiated with a specific wavelength light, hv_1, to produce a product B, which undergoes a significant change in its absorption spectrum or refractive index. Upon irradiation with another wavelength of light, hv_2, compound B reverts back to compound A, which makes it a promising candidate for the development of photoresponsive materials.[85,86] Diarylethene derivatives (DTEs) are promising organic photochromic molecules due to their excellent fatigue resistance, fast photoresponse, good heat resistance, and high isomerism yield.[87,88] DTEs can undergo ring-closure and ring-opening isomerization with different absorption spectra through photo-induced cyclization and cyclo-reduced reactions when irradiated by UV and visible light (Fig. 8B).

Similar to DTEs, spiropyran (SP) and its derivatives have also received significant attention due to their distinctive photochromic properties. When exposed to UV light, SP can be converted into cyanine (MC), resulting in a color change from colorless to blue-violet (with new absorption peaks appearing in the absorption spectrum at 550–600 nm) and a change from non-fluorescence to red fluorescence (with new emission peaks appearing at 620–750 nm). When exposed to visible light, MC quickly restores to the ring-closure SP, causing the color and fluorescence to disappear simultaneously (Fig. 8C).[89–91]

3.1.3. Photocycloaddition. Photocycloaddition reaction is a bimolecular reaction where two conjugated systems combine to form a cyclic molecule. The carbon atoms of the end groups of the two conjugated systems are attached to each other head to tail, resulting in the formation of a larger cyclic molecule. Examples of such molecules include coumarin, cinnamic acid, anthracene, and its derivatives. For instance, anthracene and its derivatives can undergo a reversible [4+4]-cycloaddition reaction under UV light irradiation, accompanied by significant photochromic behaviors (Fig. 8D).[92,93]

3.1.4. Photothermal conversion. Photothermal conversion is the process of collecting and utilizing the radiant energy of light by absorption or otherwise, and converting the energy into thermal energy and releasing it in the form of heat. Lanthanide materials exhibit high quantum efficiency and low spontaneous emission losses, rendering them an optimal material for photothermal conversion. Lanthanide complexes and Ln-UCNPs, as the typical photothermal conversion material, are able to absorb light and partially convert the energy into heat.[94,95]

3.2. Functionalities of photoresponsive molecules

3.2.1. Azobenzene. Sol–gel transition can be achieved by assembling azobenzene with α-cyclodextrins (α-CD). E-azobenzene exhibits a strong binding ability to α-CD, and undergoes isomerization to the Z-azobenzene upon UV light irradiation, causing detachment from α-CD. As a result, the
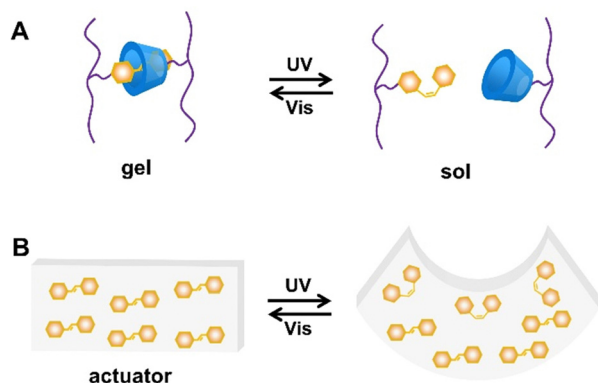

Fig. 8 Common photoresponsive molecules. (A) Azobenzene. (B) Diarylethenes. (C) Spiropyran. (D) Anthracene.

Fig. 9 Schematic illustration of (A) sol–gel transition and (B) an actuator based on *trans*/*cis* isomerization of azobenzene under UV and visible light irradiation alternately.
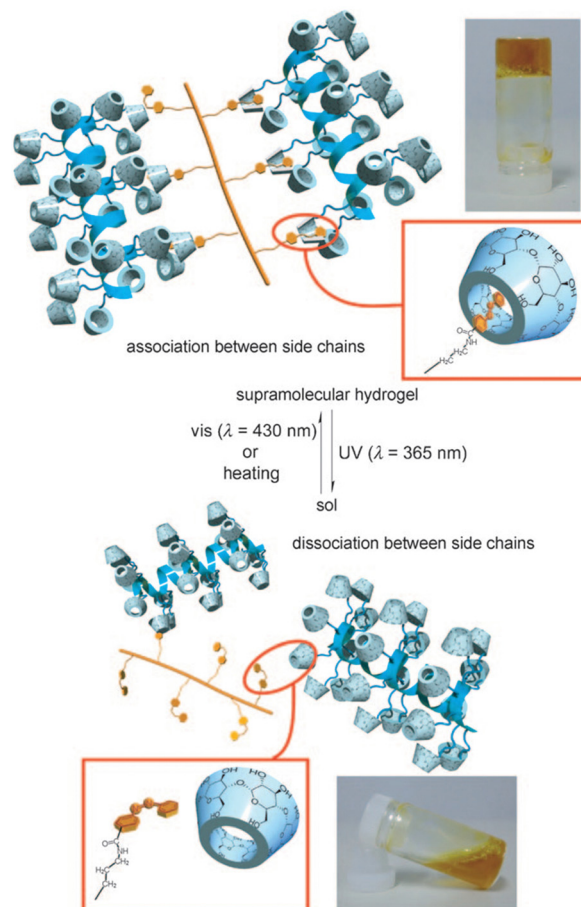

Fig. 10 Schematic illustration of sol–gel transition based on α-CD and azobenzene with UV (365 nm) and visible (430 nm) light. Reproduced with permission from ref. 96. Copyright: 2010, Wiley-VCH.

supramolecular host–guest system exhibits a reversible sol–gel transition under alternative UV and visible light irradiation by employing α-CD and azobenzene as critical cross-linking bridges (Fig. 9A).

In addition, liquid crystal systems are often prepared by introducing azobenzene to achieve photoresponsive deformation. *E*-azobenzene is a nearly rod-shaped molecule, while *Z*-azobenzene displays a curved "V" shape. The long rod-shaped *E*-azobenzene can exist as a liquid crystal radical in azobenzene-containing liquid crystal systems. After irradiating with UV light, the orderly arrangement of liquid crystal motifs can be disrupted and cause the entire liquid crystal network to macroscopically deform (Fig. 9B).

Harada *et al.* prepared supramolecular hydrogels by using α-CD modified curdlan as the backbone, which were further cross-linked with azobenzene as the guest (Fig. 10).[96] The hydrogels underwent a reversible sol–gel transition by controlling the *trans*/*cis* isomerization of azobenzene through UV/visible light irradiation alternately to modulate the dissociation and formation of α-CD/azobenzene inclusion complexes, providing a reference for the design of photoresponsive lanthanide luminescent hydrogels.

3.2.2. DTEs and SP. The UV-Vis spectra of ring-opening DTEs have no spectral overlap with the emission spectra of Ln^{3+} ions, whereas its close-form shows perfect spectral overlap with Ln^{3+} ions. Therefore, DTEs can serve as acceptors to quench or restore the luminescence of donors (Ln^{3+} ions) *via* photochromic fluorescence resonance energy transfer (FRET) (Fig. 11), which makes them promising for use in bioimaging, photoswitches, and information encryption and decryption.[97,98]

Liu *et al.* designed a host–guest system assembled by DTEs (guest molecule) and terpyridinyldibenzo-24-crown-8 as well as Eu^{3+} ions (host molecule) through noncovalent interaction (Fig. 12).[99] The UV-Vis absorption spectra of the ring-closure form of guest molecules and the luminescent emission spectra of the host molecules Eu^{3+}/terpyridinyldibenzo-24-crown-8 overlap perfectly. Furthermore, the distance between host and guest molecules is narrowed due to the host–guest interaction, which quenches the luminescence of Eu^{3+} through the FRET process. Luminescence on–off switching of the Eu^{3+} can be

effectively controlled by alternating external UV and visible light, which provided a novel design for multistage driven molecular machines and logic gates.

SP is frequently added to lanthanide luminescent systems. The luminescence of MC can be enhanced by quenching the luminescence of Ln^{3+} ions through FRET, due to the overlap between the UV-Vis absorption spectrum of MC and the emission spectrum of Ln^{3+} ions (Fig. 13). Efficient FRET between Ln^{3+} ions and SP can be used to create luminescent materials with multiple colors, providing a new idea for preparing anti-counterfeiting materials with dynamic photochromic performance.
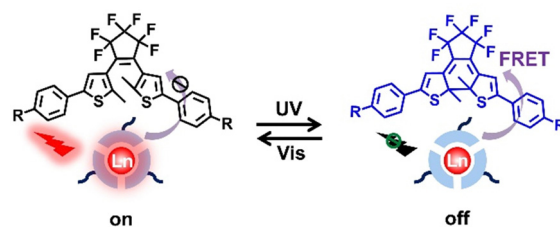

Fig. 11 Schematic illustration of luminescence on–off switching based on DTEs and lanthanide luminescent materials.
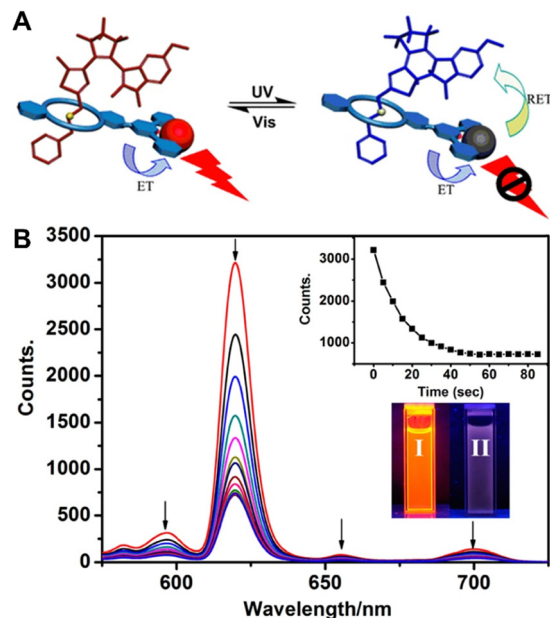
10764 | *J. Mater. Chem. C*, 2024, **12**, 10759–10774

This journal is © The Royal Society of Chemistry 2024

Fig. 12 (A) Schematic illustration of the luminescence on–off switching based on DTEs and Eu³⁺ complex. (B) Emission spectra at different times under 300 nm UV light irradiation. Insets: Emission intensity at 619 nm at different times (upper); photographs of emission color under 254 nm UV light (lower). Reproduced with permission from ref. 99. Copyright: 2013, American Chemical Society.

Fig. 14 (A) Schematic illustration of photoswitching of Ln-UCNPs/SP under 808 nm and 980 nm NIR light irradiation. (B) Emission spectra of Ln-UCNPs and the UV-Vis absorption spectra of SP and MC under 808 nm and 980 nm irradiation alternately. Reproduced with permission from ref. 100. Copyright: 2014, Wiley-VCH.

Lee *et al.* reported a core–shell structure of lanthanide-doped upconversion nanoparticles (Ln-UCNPs) (β-NaYF₄:Nd³⁺/Yb³⁺/Tm³⁺@NaYF₄:Nd³⁺@NaYF₄@NaYF₄:Yb³⁺/Er³⁺) that produced UV (347–475 nm) and visible (545 nm) emission upon excitation with NIR light at 808 and 980 nm, respectively, and then the Ln-UCNPs were further assembled with SP (Fig. 14).[100] The maximum absorption peaks of SP and MC are located at 342 nm and 560 nm, respectively, which have good overlap with the UV emission of Ln-UCNPs under 808 nm excitation and the green emission under 980 nm excitation. Therefore, this strategy achieves two-way photoswitching using dual wavelengths of NIR light.

3.2.3. Anthracene. Anthracene can act as organic ligands in lanthanide MOFs (LnMOFs) to induce a single-crystal-to-single-crystal (SC–SC) structural transition (Fig. 15). The SC–SC structural transition has attracted particular attention in the field of molecular materials chemistry and enables the creation of multifunctional materials that cannot be produced through traditional methods.[101] In addition, the process of SC–SC

structural transition can provide more structural information, leading to a better understanding of the transformation mechanism and a deeper comprehension of the relationship between structure and properties.

Zheng *et al.* synthesized a mononuclear compound Lnᴵᴵᴵ(depma)(NO₃)₃(hmpa)₂ (Ln = Dy, Gd; depma = 9-diethyl-phosphono-methylanthracene; hmpa = hexamethylphosphora-mide) using Ln³⁺ ions and anthracene derivatives (Fig. 16).[102] The face-to-face anthracene group underwent a [4+4]-cycloaddition reaction after irradiation with 365 nm UV light without loss of crystallinity, and mononuclear compounds transformed into Lnᴵᴵᴵ₂(depma₂)(NO₃)₆(hmpa)₄ dimers. Dy-containing single compounds change from single-ion to a single-molecule magnet with the luminescence color changes from yellowish-green to bluish-white, which opens up new possibilities for designing intelligent opto-magnetic devices.

3.2.4. Lanthanide complexes and Ln-UCNPs. Shape-memory polymers (SMPs) are a type of smart polymer that can be programmed to temporarily change shape and then return to their
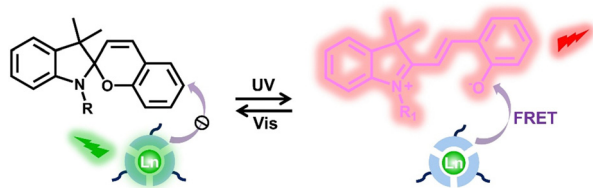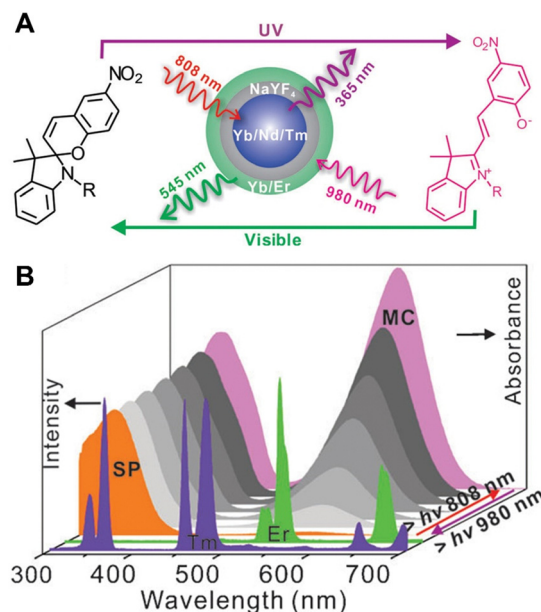

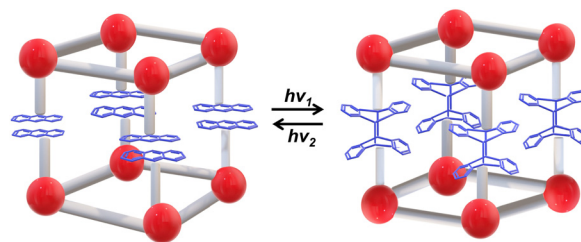Fig. 13 Schematic illustration of multicolor luminescence based on spiropyran and lanthanide luminescent materials.

Fig. 15 Schematic illustration of the photoresponsive SC–SC structural transition based on anthracene-containing LnMOFs.

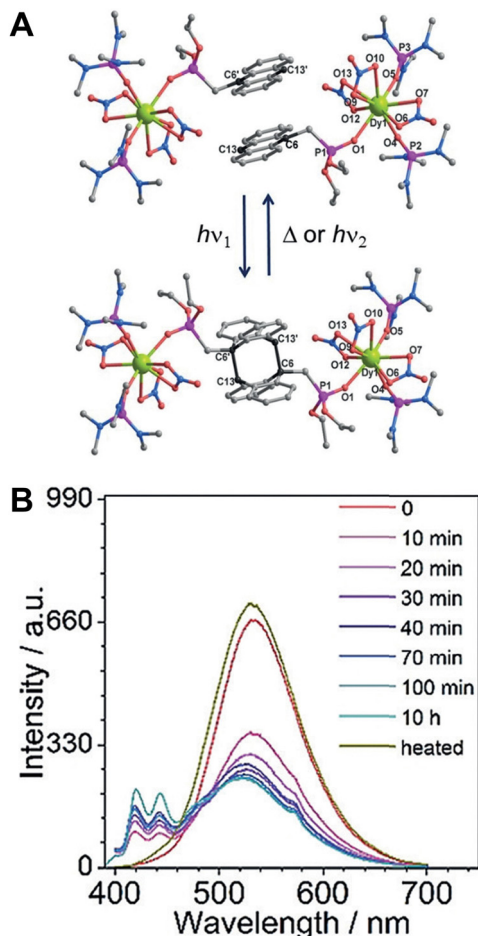This journal is © The Royal Society of Chemistry 2024

J. Mater. Chem. C, 2024, **12**, 10759–10774 | **10765**

Fig. 16 (A) Structure of $Dy^{III}(depma)(NO_3)_3(hmpa)_2$ and dimers. (B) Emission spectra of $Dy^{III}(depma)(NO_3)_3(hmpa)_2$ illuminated with 365 nm UV light at different times. Reproduced with permission from ref. 102. Copyright: 2018, Wiley-VCH.
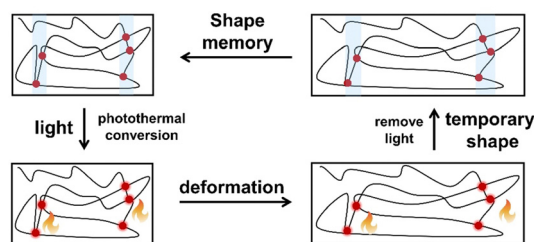

Fig. 17 Mechanism of photoresponsive SMPs: the absorption of light by Ln-UCNPs or lanthanide complexes inducing photothermal conversion and phase separation; the material can be deformed; removing light during deformation causes the material to be locked in a temporary shape; restore the material to its permanent shape with additional light irradiation and removal.

locking them in a temporary deformed state. After further UV light irradiation, the strain was released, and the material returned to its original shape.

4. Application of photoresponsive lanthanide luminescent materials

4.1. Luminescent actuators

An actuator is a material that can change its volume, shape, or position under external stimulation. These materials have attracted attention due to their potential in bionic domains, and have been used to design grippers, walkers, artificial muscles, and valves.[106–109] The integration of a photoresponse

original shape in response to specific stimuli.[103,104] Thermally induced SMPs have been extensively studied. Shape recovery can be achieved when their switching temperatures are reached through direct heating. Compared to direct heating, light has advantages as a shape-responsive stimulus source due to its remote activation, precise localization, and instantaneous switching. Lanthanide complexes and Ln-UCNPs can be utilized as photothermal fillers doped in thermally induced shape memory polymers to prepare SMP composites (Fig. 17).

Rowan *et al.* prepared metal-supramolecular polymer films with photoresponsive shape memory properties (Fig. 18).[105] Poly(butadiene) was first terminated by 4-hydroxy-2,6-bis(10-methylbenzimidazoyl)pyridine, and then cross-linked with pentaerythritol tetrakis(3-mercaptopropionate). $Eu(NTf_2)_3$ was also added during photopolymerization to prepare metal-supramolecular polymers. The Eu^{3+} complexes absorbed the UV light, and converted it into luminescence and localized heating. This caused softening of the hard phases and increased decomplexation of the Eu^{3+} complexes. As a result, the materials could be deformed under UV light. Upon removal of light, the materials cooled and the metal–ligand interactions rejoined,
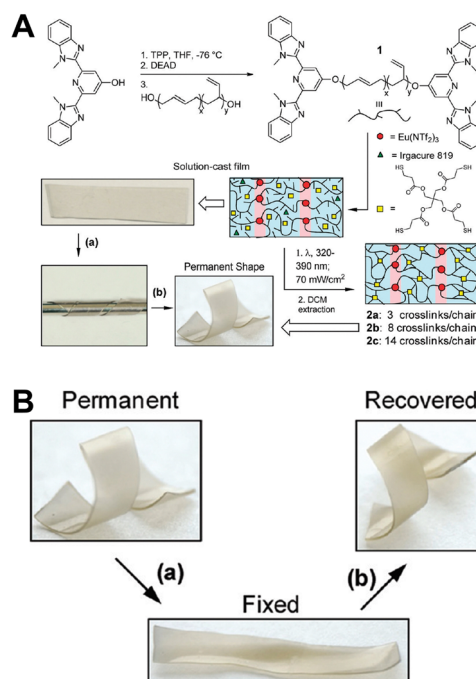

Fig. 18 (A) Chemical structure and the synthetic process of metal-supramolecular polymer films. (B) Pictures of the shape memory behavior. Reproduced with permission from ref. 105. Copyright: 2011, American Chemical Society.

10766 | *J. Mater. Chem. C*, 2024, **12**, 10759–10774

This journal is © The Royal Society of Chemistry 2024

in lanthanide luminescent systems enables the realization of their photoresponsive sol–gel transition and actuation.

Capobianco *et al.* used Ln-UCNPs that respond to NIR light to induce a sol–gel transition in supramolecular hydrogels based on azobenzene and α-CD (Fig. 19).[110] The high upconversion efficiency of Ln-UCNPs in the ultraviolet region could convert low-energy photons into high-energy UV light. This, in turn, induces the isomerization of azobenzene in the supramolecular hydrogel, leading to the dissociation of an azobenzene/α-CD inclusion complex. Therefore, the gel–sol transition was realized in this system. NIR light has excellent penetration and low cytotoxicity in biological tissues. After implantation of the hydrogel into the surgical site, the NIR light triggers the release of the guest, which can be utilized for the development of efficient and controllable drug delivery systems.

In 2018, we modified α-CD with 2,6-pyridine dicarboxylic acid (DPA) *via* a polyethylene glycol polymer chain, and then Ln^{3+} ions were added to coordinate with PDA forming a lanthanide complex. Subsequently, the guanidinium-modified azobenzene was incorporated into the lanthanide complex periphery through molecular recognition of azobenzene and α-CD, resulting in host–guest inclusion (Fig. 20).[111] Finally, a hybrid supramolecular luminescent hydrogel was constructed by the electrostatic force driving between guanidinium salts and LAPONITE® (LAP) nanosheets to form a three-dimensional network. Under UV light irradiation, *E*-azobenzene isomerizes to *Z*-azobenzene, which has greater spatial resistance, causing it to detach from the cavity of α-CD. This process cut off the cross-linking between the coordination material and the surrounding LAP nanosheets, resulting in gel–sol transition. Upon further irradiation with visible light, the *Z*-azobenzene

isomerized back to *E*-azobenzene. As a result, the azobenzene and α-CD once again formed the inclusion compound and re-cross-linked the surrounding LAP, thus initiating the transformation process from sol to gel once again. Furthermore, since the photoisomerization wavelength of azobenzene did not conflict with the excitation/emission wavelengths of lanthanide complex, the remote light-controlled gel–sol transition thus does not affect the luminescent performance of supramolecular hybrid hydrogels. In addition, the luminescence color of the hybrid hydrogel was regulated by adjusting the molar ratio of Ln^{3+} ions (Eu^{3+}/Tb^{3+}).

4.2. Photoswitches

Photoswitching materials are able to interconvert between two different light output states after being exposed to light. This property makes them a promising candidate in various fields, such as optoelectronic switching devices, molecular data processing and storage, chemical sensing, and super-resolution fluorescence microscopy.[112,113] Introducing photoresponsive molecules into lanthanide luminescent materials is an effective way to achieve luminescence on–off switching by regulating their conformation.

Liu *et al.* reported a multi-component nanosystem and explored its function as a lanthanide supramolecular

Fig. 20 (A) Schematic illustration of the sol–gel phase transition of photoresponsive hybrid luminescent supramolecular hydrogels. (B) Photographs of luminescent hydrogels with sol–gel phase transition under 254 nm UV light irradiation. Reproduced with permission from ref. 111. Copyright: 2018, Wiley-VCH.

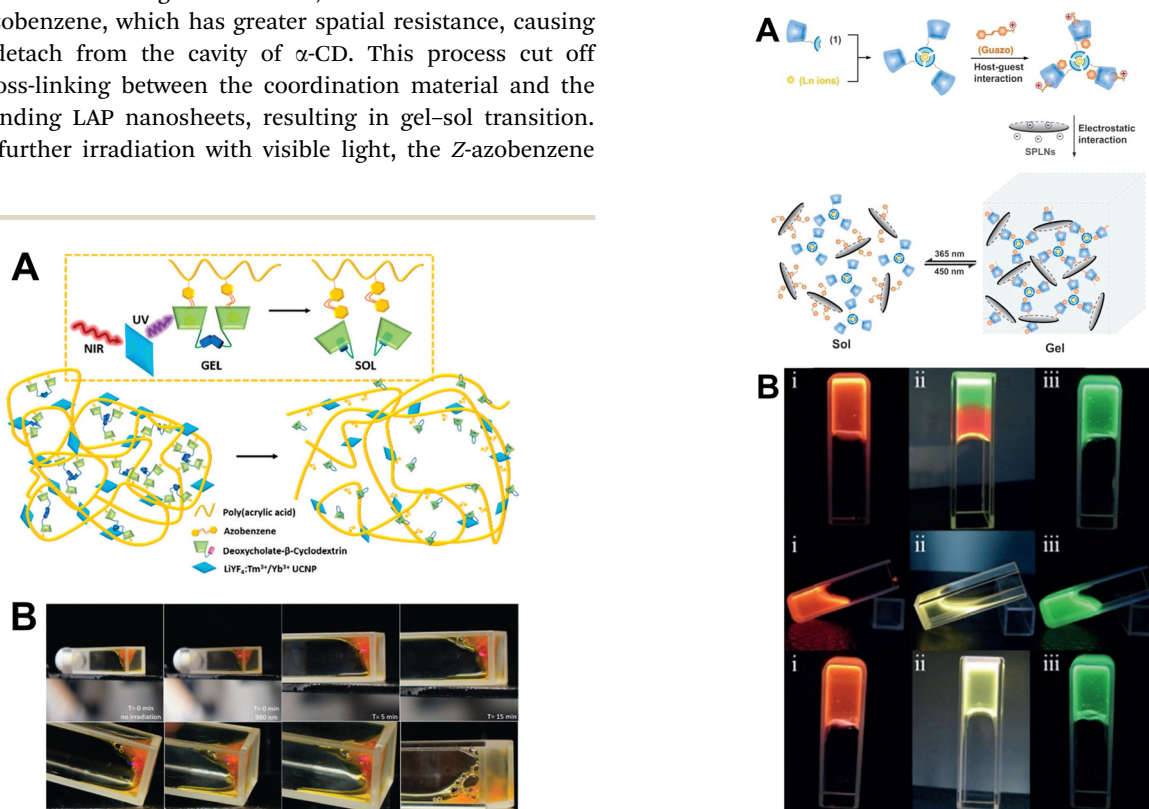Fig. 19 (A) Schematic illustration of the interactions of Ln-UCNPs, α-CD and azobenzene within the hydrogel matrix. (B) Digital photographs of gels illuminated with 980 nm NIR laser for different times. Reproduced with permission from ref. 110. Copyright: 2018, the Royal Society of Chemistry.

This journal is © The Royal Society of Chemistry 2024

J. Mater. Chem. C, 2024, **12**, 10759–10774 | **10767**

Review

View Article Online

Journal of Materials Chemistry C

photoswitch (Fig. 21A).[114] The neighbouring azobenzene units' disordered motion suppressed the lanthanide complex's luminescence. α-CD was added to immobilize the *E*-azobenzene's conformation, allowing it to display the characteristic emission of Ln^{3+} ions in both aqueous solution and hydrogel. The photoluminescence of the supramolecular lanthanide system can be modulated by alternately irradiating with UV and visible light, causing reversible association and dissociation of the α-CD/azobenzene host–guest inclusion complex. Recently, they also designed a full-color lanthanide supramolecular photoswitches, which were assembled using pyridine-2,6-dicarboxylic acid (DPA)-modified pillar[5]arene, Ln^{3+} ions, and diethylene derivatives through noncovalent interactions (Fig. 21B).[115] The supramolecular system exhibited strong luminescence emission in both organic solvents and aqueous solution due to the appropriate energy gap and strong coordination between DPA and Ln^{3+} ions. By adjusting the molar ratio of Eu^{3+}, Tb^{3+}, and host materials, the supramolecular system produced full-color emission, including white luminescence. The system's on–off luminescence can be controlled by the FRET between Ln^{3+} ions and DTEs through the ring-closure/ring-opening isomerization of diethylene. This allows for on-demand luminescence color tuning of advanced photoresponsive materials.
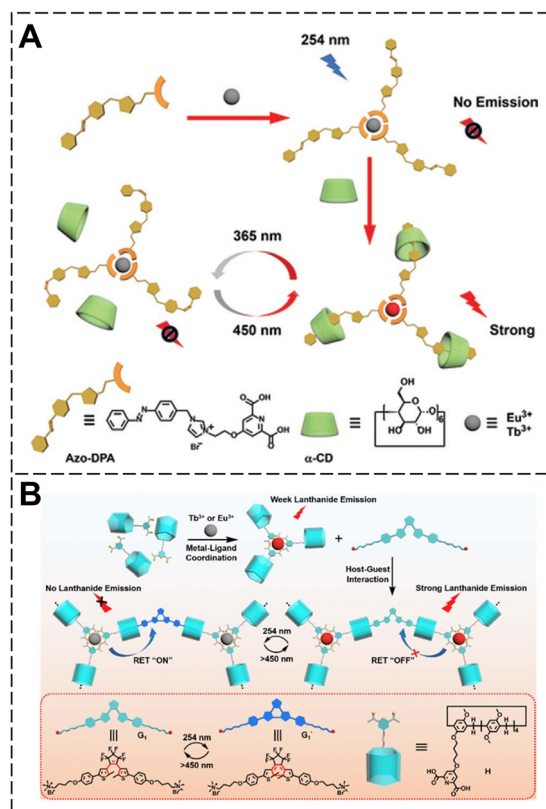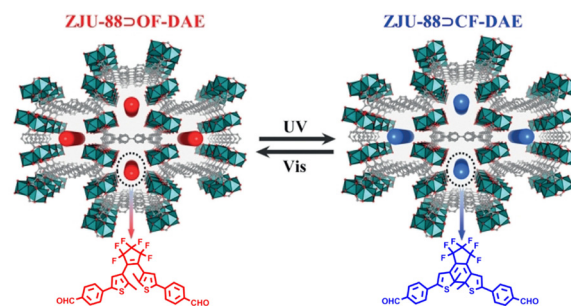
Fig. 22 Structure of LnMOFs and the molecular structures of photoresponsive DTEs. Reproduced with permission from ref. 116. Copyright: 2019, Wiley-VCH.

We reported an approach to construct photoresponsive lanthanide metal–organic frameworks (Ln-MOFs) by loading solid-state DTEs into MOFs *via* host–guest interactions, which resulted in reversible luminescence on–off photoswitching behavior through alternating UV and visible light irradiation (Fig. 22).[116] Ring-opening DTEs exhibited no absorption in the wavelength range of 400–800 nm and Ln-MOFs showed the characteristic color and brightness of Eu^{3+} ions. After irradiating with 300 nm UV light, DTEs adopted their ring-closure form and a new absorption band in the range of 500–700 nm appeared, which had good overlap with the emission spectra of Ln-MOFs, resulting in luminescence quenching due to FRET from Eu^{3+} to DTEs. When irradiated with visible light, DTE molecules switched from ring-closure form to ring-opening form, and the luminescence of LnMOFs was restored.

4.3. Intelligent anticounterfeiting

With the rapid development of social economy and technology, counterfeit and inferior goods are emerging. The counterfeiting of valuable and confidential documents, such as currency, passports, certificates, and movies, poses a significant economic and security threat to both consumers and governments.[33,117,118] Photoluminescent printing is a common means of anticounterfeiting. Many countries use anticounterfeiting labels on banknotes due to their high efficiency, facile design, and tunable optical properties. However, the use of static luminescence signals can be easily imitated, and their encrypted information can be easily decrypted.[119–121] Therefore, the design and development of high-security anti-counterfeiting materials with different luminescent colors that respond to external stimuli and change their optical outputs is of great significance in eliminating counterfeit products.

Based on Ln^{3+} ions and the photoresponse of DTEs, we constructed a series of photoresponsive lanthanide luminescent materials to be used in intelligent anticounterfeiting. The luminescence on–off switching behavior was realized by controlling the FRET from Eu^{3+} ions to DTEs by alternating UV and visible light irradiation, and potential applications in the intelligent anticounterfeiting field were further explored. In 2019, photoresponsive lanthanide luminescent hydrogels with high transparency, excellent tensile properties, and good luminescence were prepared

Fig. 21 Schematic illustration and molecular structures of lanthanide supramolecular photoswitches assembled by Ln^{3+} ions. (A) DPA-modified azobenzene and α-CD. Reproduced with permission from ref. 114. Copyright: 2022, Wiley-VCH. (B) DPA-modified pillar[5]arene and DTEs. Reproduced with permission from ref. 115. Copyright: 2023, the Royal Society of Chemistry.

10768 | *J. Mater. Chem. C*, 2024, **12**, 10759–10774

This journal is © The Royal Society of Chemistry 2024

using an *in situ* copolymerization strategy of the functionalized lanthanide complex, DTEs, and the acrylamide monomer (Fig. 23A–C).[122] Hydrogel blocks with various luminescent colors, including red, green, yellow, and colorless were arranged to form hydrogel matrix codes, allowing for the encryption and decryption of information on demand. Considering that inkjet printing is currently the most widely used printing method and the incompatibility between the printers and existing security inks due to their high viscosity or large particle content, a photoresponsive supramolecular polyelectrolyte was constructed through hierarchical self-assembly of Ln^{3+} ions, bis-ligand and DTEs driven by coordination and ionic interaction (Fig. 23D and E).[123] The supramolecular polyelectrolyte was directly utilized as an anti-counterfeiting ink in commercial printers to produce high-resolution QR codes on blue PET film, allowing for light-controlled remote multiple reversible information erasure and display. To meet different needs, multi-stimuli-responsive anisotropic hydrogels were prepared by copolymerizing magnetic alumina platelets, lanthanide complexes, DTEs, and *N*-isopropylacrylamide in a directed magnetic field.[124] The hydrogel blocks were assembled into a QR code, and the information could be hidden/recovered by UV/visible light irradiation or heating/cooling. The promising applicability in the field of multi-dimensional intelligent anti-counterfeiting could provide new research horizons for expanding the applications of functional lanthanide luminescent hydrogels.

Yang *et al.* loaded SP into LnMOFs to prepare a luminescent host–guest system for dynamic anti-counterfeiting (Fig. 24).[125] Changes in emission intensity and luminescence color can be achieved by simple UV/visible light irradiation for different times, eliminating external interfering factors. Under UV light irradiation, SP was gradually transformed into MC, which exhibited a strong absorption band at 550 nm. Energy was transferred from Ln^{3+} ions to MC through FRET, so the color of luminescence turned continuously green to red. Under visible light irradiation, MC converted back into SP, which did not overlap spectrally with Ln^{3+} ions, resulting in the cessation of FRET. Therefore, this system presented dynamic luminescent colors with prolonged irradiation time, facilitating the creation of complicated anti-counterfeiting patterns. This strategy provides novel materials to enhance the reliability of anti-counterfeiting, and practical guidance for further application in the field of dynamic anti-counterfeiting and information storage.

4.4. Theranostics

Fluorescence imaging with high sensitivity is a non-invasive method for studying biomolecular mechanisms and pathways in living cells. However, it faces challenges when applied to real samples due to the optical interference caused by the inhomogeneity of biological samples and their own fluorescence. Compared to irreversible changes in luminescence signal,
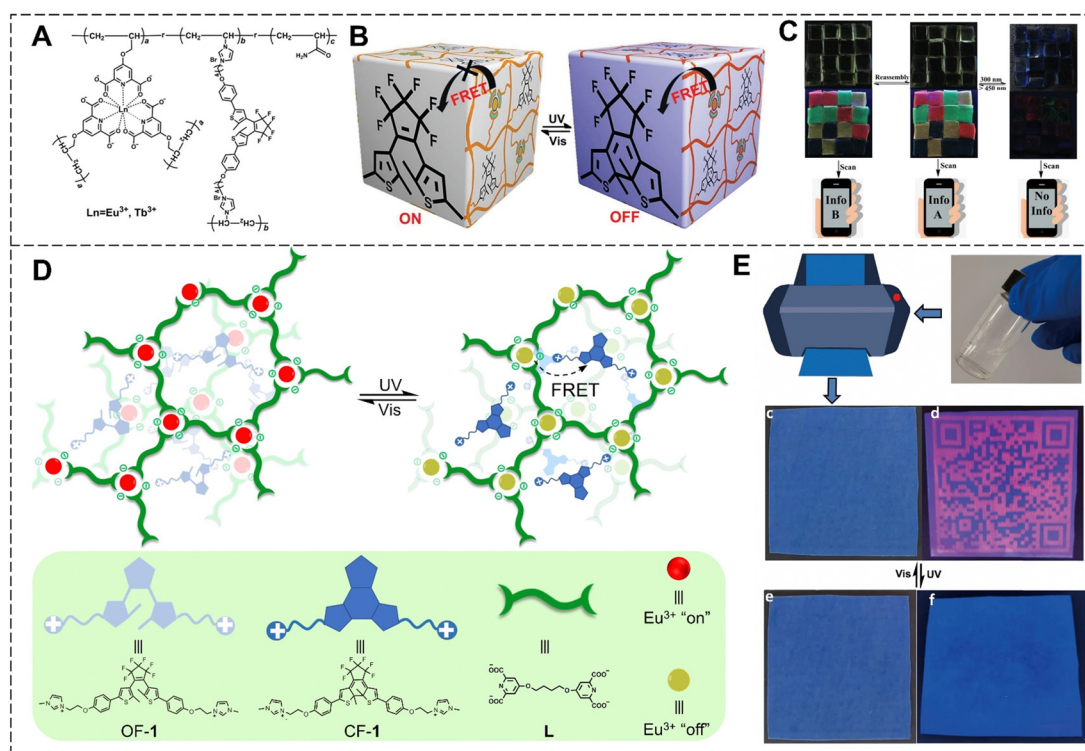

Fig. 23 (A) Chemical structure of the photoresponsive lanthanide luminescent hydrogel. (B) Schematic illustration of the luminescence on–off switching behavior by alternating UV and visible light irradiation. (C) Photos of the hydrogel matrix codes constructed by the photoresponsive hydrogel under daylight and UV light. Reproduced with permission from ref. 122. Copyright: 2019, Wiley-VCH. (D) Schematic illustration of supramolecular polyelectrolyte and chemical structures of DTEs as well as bis-ligand. (E) Schematic illustration of the printing process and photos of the QR code on blue PET film under daylight (left) and UV light (right). Reproduced with permission from ref. 123. Copyright: 2021, Nature Publishing Group.
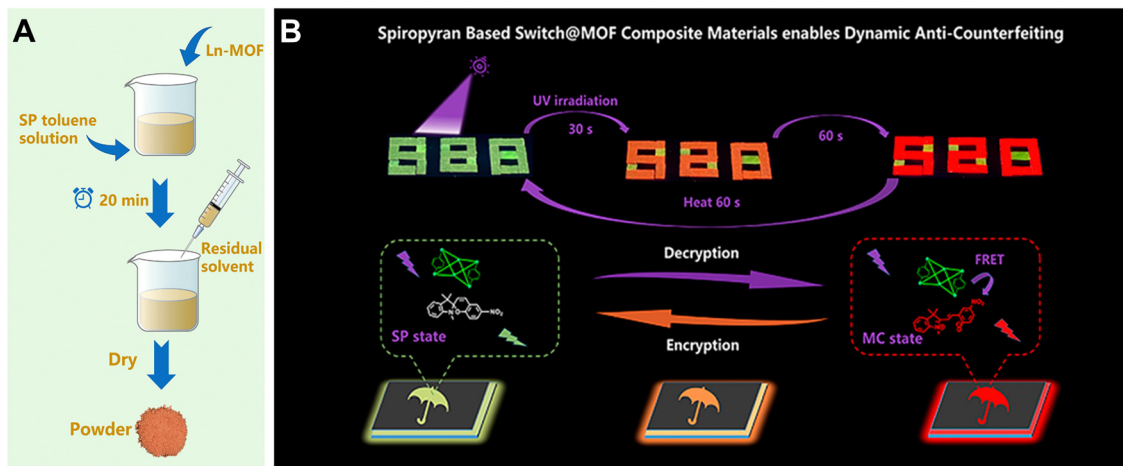
Fig. 24 (A) Synthetic process of loading SP into Tb-MOFs and (B) advanced anti-counterfeiting based on the SP@Tb-MOF/PDMS (PDMS = polydimethylsiloxane) film with a dual optical response. Reproduced with permission from ref. 125 Copyright: 2022, American Chemical Society.

luminescence that can respond reversibly provides an effective way to avoid optical interference. Therefore, designing novel luminescent probes capable of modulating the signal output is crucial for research.

Cheng et al. designed terpyridine-modified DTEs (DTE@Tpy), and coordinated them with $Eu(tta)_3 \cdot 3H_2O$ to prepare a new luminescent lanthanide molecular switch, $DTEs@TpyEu(tta)_3$. Reversible luminescence on–off switching behaviors in both solution and poly(methyl methacrylate) films were realized under external UV and visible light irradiation (Fig. 25).[126] To be noted, it can serve as a highly sensitive luminescent probe to enter living cells for imaging

Fig. 25 (A) Schematic illustration of the photoresponsive luminescence on–off switching. (B) Confocal images of NIH 3T3 cells after incubation with $CF-DTE@TpyEu(tta)_3$. Reproduced with permission from ref. 126. Copyright: 2016, American Chemical Society.

without optical interference, and luminescence on–off switching was also observed in living cells, showing potential for application in more sophisticated imaging.

In addition to being used in cell imaging, photoresponsive lanthanide luminescent materials can also be used in drug delivery platforms.[127,128] Chemotherapy remains the primary treatment for cancer. However, it can damage normal biological tissues and has a short circulation time in the body, which affects its safety and therapeutic efficacy. Light-triggered drug delivery platforms can remotely control the release of drugs at the desired location and time to realize on-demand therapy. This can significantly reduce side effects and avoid any effects toward healthy biological tissue. While most photoresponsive systems are sensitive to UV and visible light, their limited tissue penetration and photodamage restrict their further use in living systems.[129,130] Introducing NIR light-responsive Ln-UCNPs into the system can address these issues. Ln-UCNPs have the ability to absorb NIR light and convert it into UV or visible light, which can then drive the photoresponsive system to release the drug. The main mechanisms for the drug release of NIR-responsive Ln-UCNP materials are photolysis and photoisomerization.

For the photolysis strategy, photolabile molecule-coupled anticancer drugs are loaded into Ln-UCNPs. The UV/visible light emitted by Ln-UCNPs drive photolabile molecule cracking and release of anticancer drugs. Li et al. designed hydrophobic Ln-UCNPs with a core–shell structure ($NaYF_4$:Yb, $Tm@NaLuF_4$-$mSiO_2$) by photolysis (Fig. 26A).[131] They then loaded coumarin-conjugated anticancer drug chloramphenicol into the nanoparticles through physisorption. Upon 980 nm laser irradiation, the Ln-UCNPs emitted UV light, which photolytically cleaved the coumarin, releasing chloramphenicol and inhibiting tumor growth.

As another photoresponsive drug delivery platform, the photoisomerization strategy can be realized by introducing photoisomeric molecules into Ln-UCNP systems. NIR light was upconverted into UV/visible light by Ln-UCNPs. The UV/visible light triggered the photoisomerization of the photoresponsive molecules, thereby controlling the release of the drug loaded in
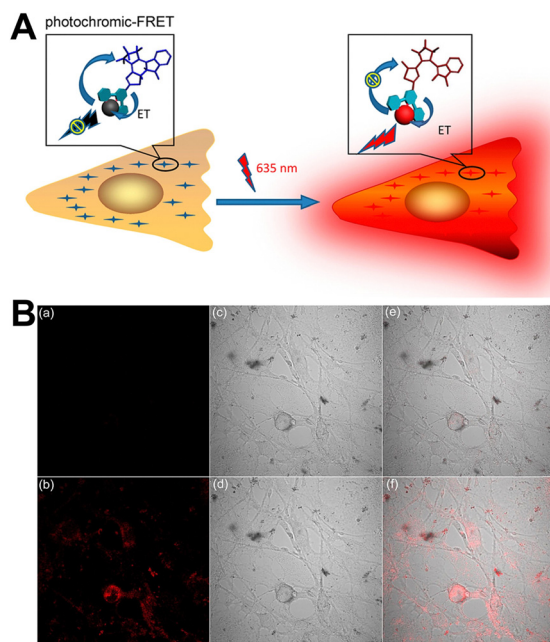
10770 | J. Mater. Chem. C, 2024, 12, 10759–10774

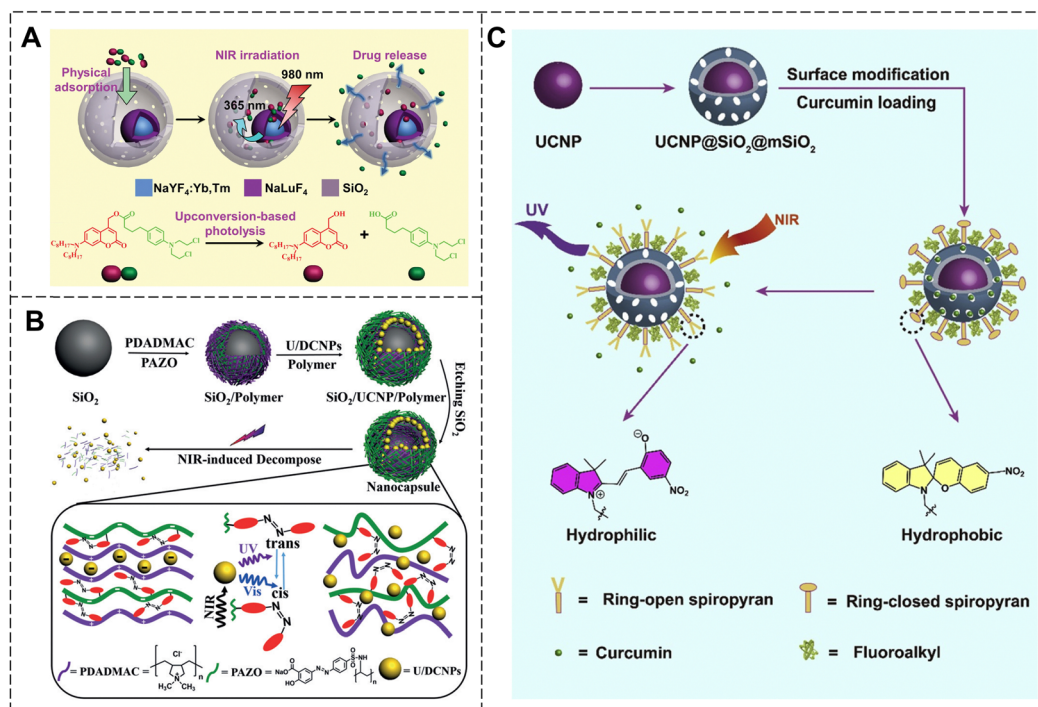This journal is © The Royal Society of Chemistry 2024

Fig. 26 (A) Schematic illustration of the NIR–responsive drug delivery and chemical structures of prodrug photolysis. Reproduced with permission from ref. 131. Copyright: 2014, Wiley-VCH. (B) The synthetic process of nanocapsules and NIR-triggered photoisomerization of azobenzene. Reproduced with permission from ref. 132. Copyright: 2018, Wiley-VCH. (C) Schematic illustration of the NIR-triggered system and photoisomerization of spiropyran. Reproduced with permission from ref. 133. Copyright: 2017, Elsevier.

the system. Zhao *et al.* modified spherical silica with positively charged polymers, and then assembled it with azobenzene-containing polymers and negatively charged dual-mode up/down-converted nanoparticles (Ln-U/DCNPs) *via* electrostatic interactions to prepare nanocapsules (Fig. 26B).[132] Under NIR light irradiation, Ln-U/DCNPs could convert NIR light into UV light. This, in turn, caused *cis/trans* isomerization of the azobenzene, leading to the decomposition of the nanocapsules and the release of the anticancer drug. Spiropyran is another photoisomeric molecule. Ring-opening SP after irradiation with visible light is hydrophobic, whereas ring-closure MC after irradiation with UV light is hydrophilic. Qu *et al.* prepared mesoporous silica-coated Ln-UCNPs, and then modified SP on the surface of silica. The hydrophobic anticancer drug curcumin was loaded into mesoporous silica (Fig. 26C).[133] Prior to NIR illumination, SP formed a dense hydrophobic layer on the surface of the silica, which prevented the premature release of curcumin. Upon NIR light irradiation, Ln-UCNPs efficiently converted NIR light into UV light, causing MC to isomerize into SP while also becoming hydrophilic, thereby enabling drug release. Additionally, the UV/visible light produced by Ln-UCNPs could activate curcumin to its triplet state and reacted with oxygen to generate reactive oxygen species, enhancing the antitumor impact.

5. Conclusions and outlook

In conclusion, this review summarizes the response mechanism, preparation method, and applications of

photoresponsive lanthanide luminescent materials in luminescent actuators, photoswitches, intelligent anticounterfeiting, and theranostics. Compared to other stimuli-responsive materials, photoresponsive lanthanide luminescent materials exhibit a number of inherent advantages, including accurate control of location and wavelength, low cost-effectiveness, and environmentally friendly nature.

This research field is rapidly evolving, with increasing emphasis on gaining a deeper understanding of the mechanism of action of photoresponsive lanthanide materials and finding simpler and more effective preparation strategies to expand their potential applications in various fields. However, challenges still exist. First, it is challenging for lanthanide luminescent materials to maintain their luminescence in aqueous environments, limiting their aqueous application, in particular in biological fields. This difficulty arises mainly due to the coupling of the high-frequency stretching vibrations of –OH in water molecules with lanthanide ions, leading to nonradiative transitions of the central lanthanide ions and luminescence quenching. Maintaining the aqueous phase luminescence of lanthanide materials often requires the elaborate design of organic ligands to increase the coordination number thus protect the lanthanide ions from water molecules. In terms of the chemical structure of ligands, it is possible to design polydentate chelating ligands, which can enhance the luminescence in aqueous solution by using synergistic coordination. Furthermore, the coordination number and structure of lanthanide complexes should also be investigated in-depth.

Alternatively, some amphiphilic ligands can be utilized to prepare complexes that can self-assemble into micelles in aqueous solution to protect the lanthanide luminescence center. Secondly, the majority of current photoresponsive lanthanide luminescent materials are driven by UV/visible light. This makes it difficult to penetrate biological tissues, can cause damage to the tissues, and they can be interfered with by the self-fluorescence of the biological tissues. The assembly of lanthanide-doped upconversion nanoparticles with photoresponsive molecules to prepare composites that utilize the energy of lanthanide-doped upconversion nanoparticles to drive photoresponsive molecules is a growing area of research. Lanthanide-doped upconversion nanoparticles are capable of converting NIR light into UV and visible light, thereby enabling the delivery and controlled release of guest molecules. Thirdly, although lanthanide luminescent materials have demonstrated effective intelligent anticounterfeiting properties, their long response time (seconds or even minutes) is still far from the requirements of actual applications. Shorter times are necessary to meet future equipment needs. Efforts are being made to investigate the potential of new photoresponsive molecules and mechanisms, or to modify existing photoresponsive molecules. In parallel, efforts can be made to enhance the understanding of the relationship between suitable structures and photoresponse by integrating theoretical calculations into the structural design and synthesis of materials. This approach could facilitate more effective and precise control over the resulting materials.

Author contributions

All authors have given approval to the final version of the manuscript. Lingna Su: data curation and writing – original draft; Xiao Liu: conceptualization (table of contents) and writing – original draft; Qingyu Niu: data curation (sensing mechanisms) and writing – original draft; and Zhiqiang Li: funding acquisition, data validation, and writing – reviewing and editing.

Conflicts of interest

The authors have no conflicts of interest.

Acknowledgements

Notes and references

1 J.-C. G. Bünzli, *Acc. Chem. Res.*, 2006, **39**, 53–61.
2 J.-C. G. Bünzli and S. V. Eliseeva, *Chem. Sci.*, 2013, **4**, 1939–1949.
3 M. C. Heffern, L. M. Matosziuk and T. J. Meade, *Chem. Rev.*, 2014, **114**, 4496–4539.
4 X.-Z. Li, C.-B. Tian and Q.-F. Sun, *Chem. Rev.*, 2022, **122**, 6374–6458.
5 X. Qin, X. Liu, W. Huang, M. Bettinelli and X. Liu, *Chem. Rev.*, 2017, **117**, 4488–4527.
6 Y. Liu, D. Tu, H. Zhu and X. Chen, *Chem. Soc. Rev.*, 2013, **42**, 6924–6958.
7 E. G. Moore, A. P. S. Samuel and K. N. Raymond, *Acc. Chem. Res.*, 2009, **42**, 542–552.
8 D. Chen, Y. Wang and M. Hong, *Nano Energy*, 2012, **1**, 73–90.
9 G. Wang, Q. Peng and Y. Li, *Acc. Chem. Res.*, 2011, **44**, 322–332.
10 P. Singh, S. Kachhap, P. Singh and S. K. Singh, *Coord. Chem. Rev.*, 2022, **472**, 214795.
11 L. Armelao, S. Quici, F. Barigelletti, G. Accorsi, G. Bottaro, M. Cavazzini and E. Tondello, *Coord. Chem. Rev.*, 2010, **254**, 487–505.
12 E. R. Trivedi, S. V. Eliseeva, J. Jankolovits, M. M. Olmstead, S. Petoud and V. L. Pecoraro, *J. Am. Chem. Soc.*, 2014, **136**, 1526–1534.
13 J.-C. G. Bünzli, *Trends Chem.*, 2019, **1**, 751–762.
14 J. Feng and H. Zhang, *Chem. Soc. Rev.*, 2013, **42**, 387–410.
15 S.-J. Li, F. Li, N. Kong, J.-R. Liu and X. Zhu, *Adv. Healthcare Mater.*, 2023, **12**, 2302276.
16 Z. Wang, M. Zhang, S. Chi, M. Zhu, C. Wang and Z. Liu, *Adv. Healthcare Mater.*, 2022, **11**, 2200521.
17 J. Xu, A. Gulzar, P. Yang, H. Bi, D. Yang, S. Gai, F. He, J. Lin, B. Xing and D. Jin, *Coord. Chem. Rev.*, 2019, **381**, 104–134.
18 P. Du, R. An, Y. Liang, P. Lei and H. Zhang, *Coord. Chem. Rev.*, 2022, **471**, 214745.
19 K. Binnemans, *Chem. Rev.*, 2009, **109**, 4283–4374.
20 A. A. Ansari, M. R. Muthumareeswaran and R. Lv, *Coord. Chem. Rev.*, 2022, **466**, 214584.
21 S. Weissman, *J. Chem. Phys.*, 1942, **10**, 214–217.
22 D. E. Barry, D. F. Caffrey and T. Gunnlaugsson, *Chem. Soc. Rev.*, 2016, **45**, 3244–3274.
23 P. A. Vigato, V. Peruzzo and S. Tamburini, *Coord. Chem. Rev.*, 2009, **253**, 1099–1201.
24 K. Miyata, Y. Konno, T. Nakanishi, A. Kobayashi, M. Kato, K. Fushimi and Y. Hasegawa, *Angew. Chem., Int. Ed.*, 2013, **52**, 6413–6416.
25 Z. Li, Z. Hou, H. Fan and H. Li, *Adv. Funct. Mater.*, 2017, **27**, 1604379.
26 Q. Zhu, L. Zhang, K. Van Vliet, A. Miserez and N. Holten-Andersen, *ACS Appl. Mater. Interfaces*, 2018, **10**, 10409–10418.
27 Z. Gao, B. Xu, T. Zhang, Z. Liu, W. Zhang, X. Sun, Y. Liu, X. Wang, Z. Wang and Y. Yan, *Angew. Chem., Int. Ed.*, 2020, **59**, 19060–19064.
28 J.-C. G. Bünzli and C. Piguet, *Chem. Soc. Rev.*, 2005, **34**, 1048–1077.
29 P. Li and H. Li, *Coord. Chem. Rev.*, 2021, **441**, 213988.
30 H.-Q. Yin, X.-Y. Wang and X.-B. Yin, *J. Am. Chem. Soc.*, 2019, **141**, 15166–15173.
31 K. Wu, X.-Y. Liu, Y.-L. Huang, M. Xie, X. Xiong, J. Zheng, W. Lu and D. Li, *Inorg. Chem. Front.*, 2022, **9**, 1714–1721.

10772 | *J. Mater. Chem. C*, 2024, **12**, 10759–10774

This journal is © The Royal Society of Chemistry 2024

32 J. Zhuang, M. R. Gordon, J. Ventura, L. Li and S. Thayumanavan, *Chem. Soc. Rev.*, 2013, **42**, 7421–7435.

33 M.-K. Tsang, G. Bai and J. Hao, *Chem. Soc. Rev.*, 2015, **44**, 1585–1607.

34 X. He, J. Wang, X. Liu, Q. Niu, Z. Li, B. Chen and Q. Xiong, *Adv. Healthcare Mater.*, 2024, 2400747.

35 R. Gao, X. Fang and D. Yan, *J. Mater. Chem. C*, 2019, **7**, 3399–3412.

36 M. Radisic, H. Park, H. Shing, T. Consi, F. J. Schoen, R. Langer, L. E. Freed and G. Vunjak-Novakovic, *Proc. Natl. Acad. Sci. U. S. A.*, 2004, **101**, 18129–18134.

37 M.-C. Wong, L. Chen, G. Bai, L.-B. Huang and J. Hao, *Adv. Mater.*, 2017, **29**, 1701945.

38 F. Yang, Y. Yuan, R. P. Sijbesma and Y. Chen, *Macromolecules*, 2020, **53**, 905–912.

39 Y. Gao, P. Jing, N. Yan, M. Hilbers, H. Zhang, G. Rothenberg and S. Tanase, *Chem. Commun.*, 2017, **53**, 4465–4468.

40 T. Feng, Y. Ye, X. Liu, H. Cui, Z. Li, Y. Zhang, B. Liang, H. Li and B. Chen, *Angew. Chem., Int. Ed.*, 2020, **59**, 21752–21757.

41 X. Liu, B. Li, Y. Xu, Z. Li, Y. Zhang, Z.-J. Ding, H. Cui, J. Wang, H.-B. Hou and H. Li, *Dalton Trans.*, 2019, **48**, 7714–7719.

42 X. Zhang, K. Jiang, H. He, D. Yue, D. Zhao, Y. Cui, Y. Yang and G. Qian, *Sens. Actuators, B*, 2018, **254**, 1069–1077.

43 Z. Dai, L. Tian, B. Song, Z. Ye, X. Liu and J. Yuan, *Anal. Chem.*, 2014, **86**, 11883–11889.

44 L. Lu, C. Chen, D. Zhao, J. Sun and X. Yang, *Anal. Chem.*, 2016, **88**, 1238–1245.

45 P. Chen, Q. Li, S. Grindy and N. Holten-Andersen, *J. Am. Chem. Soc.*, 2015, **137**, 11590–11593.

46 X. Li, Y. Xie, B. Song, H.-L. Zhang, H. Chen, H. Cai, W. Liu and Y. Tang, *Angew. Chem., Int. Ed.*, 2017, **56**, 2689–2693.

47 Y. Liu, Z. Wei, X. Liao and J. Zhou, *Acc. Mater. Res.*, 2020, **1**, 225–235.

48 J.-C. G. Bünzli, *Chem. Rev.*, 2010, **110**, 2729–2755.

49 B. Yan, *Acc. Chem. Res.*, 2017, **50**, 2789–2798.

50 D. Parker, J. D. Fradgley and K.-L. Wong, *Chem. Soc. Rev.*, 2021, **50**, 8193–8213.

51 H. Liu, S. Wei, H. Qiu, M. Si, G. Lin, Z. Lei, W. Lu, L. Zhou and T. Chen, *Adv. Funct. Mater.*, 2022, **32**, 2108830.

52 X. Feng, C. Wang, S. Shang, H. Liu, X. Huang, J. Jiang and H. Zhang, *Chem. Eng. J.*, 2022, **450**, 138356.

53 Y. Xie, G. Sun, J. Li and L. Sun, *Adv. Funct. Mater.*, 2023, **33**, 2303663.

54 L. E. MacKenzie and R. Pal, *Nat. Rev. Chem.*, 2021, **5**, 109–124.

55 Q. Xiao, X. Yin, L. Lv, X. Dong, N. Zhou, K. Liu and X. Luo, *J. Rare Earths*, 2023, **41**, 981–988.

56 M. M. Upadhyay and K. Kumar, *J. Rare Earths*, 2023, **41**, 1295–1301.

57 X. Liu, Y. Ye, X. He, Q. Niu, B. Chen and Z. Li, *Angew. Chem., Int. Ed.*, 2024, **63**, e202400195.

58 Y. Cui, H. Xu, Y. Yue, Z. Guo, J. Yu, Z. Chen, J. Gao, Y. Yang, G. Qian and B. Chen, *J. Am. Chem. Soc.*, 2012, **134**, 3979–3982.

59 B. Li, Z. Song, K. Zhu, Q. Niu, Z. Li and H. Li, *ACS Appl. Mater. Interfaces*, 2021, **13**, 20633–20640.

60 W.-M. Liu, P. H. J. Keizers, M. A. S. Hass, A. Blok, M. Timmer, A. J. C. Sarris, M. Overhand and M. Ubbink, *J. Am. Chem. Soc.*, 2012, **134**, 17306–17313.

61 D. Mouchel Dit Leguerrier, R. Barré, J. K. Molloy and F. Thomas, *Coord. Chem. Rev.*, 2021, **446**, 214133.

62 W.-L. Chan, C. Xie, W.-S. Lo, J.-C. G. Bünzli, W.-K. Wong and K.-L. Wong, *Chem. Soc. Rev.*, 2021, **50**, 12189–12257.

63 A. R. Lippert, T. Gschneidtner and C. J. Chang, *Chem. Commun.*, 2010, **46**, 7510–7512.

64 B. Li, Z.-J. Ding, Z. Li and H. Li, *J. Mater. Chem. C*, 2018, **6**, 6869–6874.

65 X. Liu, B. Li, W. Wang, Z. Li and Q. Xiong, *Inorg. Chem. Front.*, 2022, **9**, 4194–4200.

66 Z. Liu, W. He and Z. Guo, *Chem. Soc. Rev.*, 2013, **42**, 1568–1600.

67 G. Weng, S. Thanneeru and J. He, *Adv. Mater.*, 2018, **30**, 1706526.

68 L. K. Truman, S. Comby and T. Gunnlaugsson, *Angew. Chem., Int. Ed.*, 2012, **51**, 9624–9627.

69 S.-L. Hou, J. Dong, M.-H. Tang, X.-L. Jiang, Z.-H. Jiao and B. Zhao, *Anal. Chem.*, 2019, **91**, 5455–5460.

70 D. Zhao, J. Yang, X. Tian, J. Wei, Q. Li and Y. Wang, *Chem. Eng. J.*, 2022, **434**, 134806.

71 K. Luan, R. Meng, C. Shan, J. Cao, J. Jia, W. Liu and Y. Tang, *Anal. Chem.*, 2018, **90**, 3600–3607.

72 Y. Zhou, H. Ye, Y. Chen, R. Zhu and L. Yin, *Biomacromolecules*, 2018, **19**, 1840–1857.

73 Y. Sun, Y. Sha, G. Cui, F. Meng and Z. Zhong, *Adv. Drug Delivery Rev.*, 2023, **192**, 114624.

74 X. Sun, J. Sun, B. Dong, G. Huang, L. Zhang, W. Zhou, J. Lv, X. Zhang, M. Liu, L. Xu, X. Bai, W. Xu, Y. Yang, X. Song and H. Song, *Biomaterials*, 2019, **201**, 42–52.

75 R. M. Supkowski, J. P. Bolender, W. D. Smith, L. E. L. Reynolds and W. D. Horrocks Jr, *Coord. Chem. Rev.*, 1999, **185–186**, 307–319.

76 X. Liu, Z. Tang, B. Song, H. Ma and J. Yuan, *J. Mater. Chem. B*, 2017, **5**, 2849–2855.

77 M. Burnworth, L. Tang, J. R. Kumpfer, A. J. Duncan, F. L. Beyer, G. L. Fiore, S. J. Rowan and C. Weder, *Nature*, 2011, **472**, 334–337.

78 J. Zhang and H. Tian, *Adv. Opt. Mater.*, 2018, **6**, 1701278.

79 H. M. D. Bandara and S. C. Burdette, *Chem. Soc. Rev.*, 2012, **41**, 1809–1825.

80 L. Kortekaas and W. R. Browne, *Chem. Soc. Rev.*, 2019, **48**, 3406–3424.

81 S. Fredrich, R. Göstl, M. Herder, L. Grubert and S. Hecht, *Angew. Chem., Int. Ed.*, 2016, **55**, 1208–1212.

82 B. Slepetz and M. Kertesz, *J. Am. Chem. Soc.*, 2013, **135**, 13720–13727.

83 J. Fregoni, G. Granucci, E. Coccia, M. Persico and S. Corni, *Nat. Commun.*, 2018, **9**, 4688.

84 D.-Y. Kim, W.-J. Yoon, Y.-J. Choi, S.-I. Lim, J. Koo and K.-U. Jeong, *J. Mater. Chem. C*, 2018, **6**, 12314–12320.

85 M. Irie, *Chem. Rev.*, 2000, **100**, 1683–1684.

86 L. Wang and Q. Li, *Chem. Soc. Rev.*, 2018, **47**, 1044–1097.

87 T. Fukaminato, T. Sasaki, T. Kawai, N. Tamai and M. Irie, *J. Am. Chem. Soc.*, 2004, **126**, 14843–14849.

88 H. Miyasaka, M. Murakami, A. Itaya, D. Guillaumont, S. Nakamura and M. Irie, *J. Am. Chem. Soc.*, 2001, **123**, 753–754.

89 H.-Q. Zheng, Y. Yang, Z. Wang, D. Yang, G. Qian and Y. Cui, *Adv. Mater.*, 2023, **35**, 2300177.

90 Z. He, Y. Li, H. Wu, Y. Yang, Y. Chen, J. Zhu, Q. Li and G. Jiang, *ACS Appl. Mater. Interfaces*, 2022, **14**, 48133–48142.

91 Z. Zhang, X. Kang, X. Zhao, X. Dai, X. Su, B. Yang, Y. Luo, C. Xiong, H. Chang and X. Li, *J. Mater. Chem. C*, 2024, **12**, 5191–5202.

92 J. H. Kim, S. V. Lindeman and J. K. Kochi, *J. Am. Chem. Soc.*, 2001, **123**, 4951–4959.

93 M. Li, A. D. Schlüter and J. Sakamoto, *J. Am. Chem. Soc.*, 2012, **134**, 11721–11725.

94 H. Wang, L. Fang, Z. Zhang, J. Epaarachchi, L. Li, X. Hu, C. Lu and Z. Xu, *Composites, Part A*, 2019, **125**, 105525.

95 L. Fang, T. Fang, X. Liu, Y. Ni, C. Lu and Z. Xu, *Compos. Sci. Technol.*, 2017, **152**, 190–197.

96 S. Tamesue, Y. Takashima, H. Yamaguchi, S. Shinkai and A. Harada, *Angew. Chem., Int. Ed.*, 2010, **49**, 7461–7464.

97 T. M. Khang, P. Q. Nhien, T. T. K. Cuc, C.-C. Weng, C.-H. Wu, J. I. Wu, B. T. B. Hue, Y.-K. Li and H.-C. Lin, *Small*, 2023, **19**, 2205597.

98 S. Lin, K. G. Gutierrez-Cuevas, X. Zhang, J. Guo and Q. Li, *Adv. Funct. Mater.*, 2021, **31**, 2007957.

99 H.-B. Cheng, H.-Y. Zhang and Y. Liu, *J. Am. Chem. Soc.*, 2013, **135**, 10190–10193.

100 J. Lai, Y. Zhang, N. Pasquale and K.-B. Lee, *Angew. Chem., Int. Ed.*, 2014, **53**, 14419–14423.

101 S.-L. Huang, T. A. Hor and G.-X. Jin, *Coord. Chem. Rev.*, 2017, **346**, 112–122.

102 X.-D. Huang, Y. Xu, K. Fan, S.-S. Bao, M. Kurmoo and L.-M. Zheng, *Angew. Chem., Int. Ed.*, 2018, **57**, 8577–8581.

103 A. Lendlein and S. Kelch, *Angew. Chem., Int. Ed.*, 2002, **41**, 2034–2057.

104 M. Behl and A. Lendlein, *Mater. Today*, 2007, **10**, 20–28.

105 J. R. Kumpfer and S. J. Rowan, *J. Am. Chem. Soc.*, 2011, **133**, 12866–12874.

106 H. Yuk, S. Lin, C. Ma, M. Takaffoli, N. X. Fang and X. Zhao, *Nat. Commun.*, 2017, **8**, 14230.

107 C. Ma, X. Le, X. Tang, J. He, P. Xiao, J. Zheng, H. Xiao, W. Lu, J. Zhang, Y. Huang and T. Chen, *Adv. Funct. Mater.*, 2016, **26**, 8670–8676.

108 C.-H. Zhu, Y. Lu, J. Peng, J.-F. Chen and S.-H. Yu, *Adv. Funct. Mater.*, 2012, **22**, 4017–4022.

109 S. Wei, W. Lu, X. Le, C. Ma, H. Lin, B. Wu, J. Zhang, P. Theato and T. Chen, *Angew. Chem., Int. Ed.*, 2019, **58**, 16243–16251.

110 G. A. Mandl, P. A. Rojas-Gutierrez and J. A. Capobianco, *Chem. Commun.*, 2018, **54**, 5847–5850.

111 Z. Li, G. Wang, Y. Wang and H. Li, *Angew. Chem., Int. Ed.*, 2018, **57**, 2194–2198.

112 M.-M. Russew and S. Hecht, *Adv. Mater.*, 2010, **22**, 3348–3360.

113 J. Volarić, W. Szymanski, N. A. Simeth and B. L. Feringa, *Chem. Soc. Rev.*, 2021, **50**, 12377–12449.

114 H.-J. Yu, H. Wang, F.-F. Shen, F.-Q. Li, Y.-M. Zhang, X. Xu and Y. Liu, *Small*, 2022, **18**, 2201737.

115 W.-L. Zhou, X.-Y. Dai, W. Lin, Y. Chen and Y. Liu, *Chem. Sci.*, 2023, **14**, 6457–6466.

116 Z. Li, G. Wang, Y. Ye, B. Li, H. Li and B. Chen, *Angew. Chem., Int. Ed.*, 2019, **58**, 18025–18031.

117 S. Shikha, T. Salafi, J. Cheng and Y. Zhang, *Chem. Soc. Rev.*, 2017, **46**, 7054–7093.

118 P. Kumar, S. Singh and B. K. Gupta, *Nanoscale*, 2016, **8**, 14297–14340.

119 F. Li, X. Wang, Z. Xia, C. Pan and Q. Liu, *Adv. Funct. Mater.*, 2017, **27**, 1700051.

120 X. Ji, R.-T. Wu, L. Long, X.-S. Ke, C. Guo, Y.-J. Ghang, V. M. Lynch, F. Huang and J. L. Sessler, *Adv. Mater.*, 2018, **30**, 1705480.

121 X. Chen, Q. Jin, L. Wu, C. Tung and X. Tang, *Angew. Chem., Int. Ed.*, 2014, **53**, 12542–12547.

122 Z. Li, H. Chen, B. Li, Y. Xie, X. Gong, X. Liu, H. Li and Y. Zhao, *Adv. Sci.*, 2019, **6**, 1901529.

123 Z. Li, X. Liu, G. Wang, B. Li, H. Chen, H. Li and Y. Zhao, *Nat. Commun.*, 2021, **12**, 1363.

124 X. Liu, B. Li, W. Wang, Y. Zhang, H. Li and Z. Li, *Chem. Eng. J.*, 2022, **449**, 137718.

125 Y. Yang, Y. Li, Y. Chen, Z. Wang, Z. He, J. He and H. Zhao, *ACS Appl. Mater. Interfaces*, 2022, **14**, 21330–21339.

126 H.-B. Cheng, G.-F. Hu, Z.-H. Zhang, L. Gao, X. Gao and H.-C. Wu, *Inorg. Chem.*, 2016, **55**, 7962–7968.

127 W. Zhao, Y. Zhao, Q. Wang, T. Liu, J. Sun and R. Zhang, *Small*, 2019, **15**, 1903060.

128 T. Zhao, L. Chen, Q. Li and X. Li, *J. Mater. Chem. B*, 2018, **6**, 7112–7121.

129 Y.-P. Gu, R. Cui, Z.-L. Zhang, Z.-X. Xie and D.-W. Pang, *J. Am. Chem. Soc.*, 2012, **134**, 79–82.

130 J. Yan, B. Li, P. Yang, J. Lin and Y. Dai, *Adv. Funct. Mater.*, 2021, **31**, 2104325.

131 L. Zhao, J. Peng, Q. Huang, C. Li, M. Chen, Y. Sun, Q. Lin, L. Zhu and F. Li, *Adv. Funct. Mater.*, 2014, **24**, 363–371.

132 T. Zhao, P. Wang, Q. Li, A. A. Al-Khalaf, W. N. Hozzein, F. Zhang, X. Li and D. Zhao, *Angew. Chem., Int. Ed.*, 2018, **57**, 2611–2615.

133 C. Liu, Y. Zhang, M. Liu, Z. Chen, Y. Lin, W. Li, F. Cao, Z. Liu, J. Ren and X. Qu, *Biomaterials*, 2017, **139**, 151–162.

10774 | *J. Mater. Chem. C*, 2024, **12**, 10759–10774

This journal is © The Royal Society of Chemistry 2024